Enhanced power factor in the promising thermoelectric material $SnPb_xTe$ prepared *via* zone-melting†

Jun He,[ab] Jingtao Xu,*[a] Guoqiang Liu,[a] Xiaojian Tan,[a] Hezhu Shao,[a] Zhu Liu,[a] Jiaqiang Xu,*[b] Jun Jiang[a] and Haochuan Jiang[a]

Tin telluride (SnTe) has recently attracted much attention as a promising thermoelectric material. In this work, SnTe is alloyed with additional Pb, and the high density crystalline ingots of $SnPb_xTe$ ($x = 0$, 0.02, 0.04, and 0.06) have been synthesized by a zone-melting method. Through this method, $SnPb_xTe$ samples show larger power factors than those prepared by other methods, and a maximum value of 30.5 μW cm^{-1} K^{-2} at 823 K has been reached in p-type $SnPb_{0.02}Te$, which is the highest value reported so far. As a result, a promising figure of merit ZT of ~0.81 has been obtained at 823 K.

Introduction

Thermoelectric materials have attracted wide attention due to their potential applications in future energy generation.[1–3] The conversion efficiency is governed by the non-dimensional figure of merit, defined as $ZT = S^2\sigma T/\kappa$, where S, σ, T, and κ are the Seebeck coefficient, the electrical conductivity, the absolute temperature, and the thermal conductivity, respectively. To optimize thermoelectric performance, a large power factor $S^2\sigma$ and low thermal conductivity should be obtained at the same time.[4] Attempts to increase the power factor include enhancement of the Seebeck coefficient through carrier engineering, convergence of degenerate electronic band valleys, and the formation of resonance levels in the electronic bands. The reduction of the thermal conductivity have been achieved through phonon scattering by solid solution point defects, second phase nano-precipitates, mesoscale grain boundaries, and intrinsic bond anharmonicity.[5]

Lead chalcogenide and its alloys exhibit high ZT values in the middle temperature range.[4,6] However, their applications have been limited by the concern about the toxic element Pb. SnTe, a homologue of PbTe, has the potential to be a good thermoelectric material due to its similar band characteristic to PbTe.[7,8] Previous studies show that SnTe has many intrinsic vacancies, leading to a very high carrier concentration.[9–11] Therefore, SnTe shows low S and high κ, resulting in a very poor thermoelectric performance.

To enhance the thermoelectric performance, SnTe has been alloyed with other metal tellurides such as AgSbTe, $AgBiTe_2$.[12,13] Through In doping, the Seebeck coefficient of SnTe has been significantly enhanced due to the formation of resonance levels in the valence band, resulting in a ZT of ~1.1 at 873 K.[10] Through iodine doping, the carrier concentration in the light valence band of SnTe was effectively tuned, which essentially tunes the thermoelectric properties. Se doping was used to reduce the lattice thermal conductivity of SnTe, and with the resonance level by In doping, a ZT of 0.8 is obtained in $SnTe_{0.85}Se_{0.15}$:In.[14] Recently, G. J. Tan *et al.* reported that Sn self-compensation can effectively reduce the Sn vacancies and decrease the hole carrier density.[11] As a result, the ZT is improved by 50%. With further modification of the band structure by Cd, Hg, or Mg alloying in SnTe, the Seebeck coefficient of SnTe is greatly enhanced and the maximum ZT value is larger than 1.2 above 860 K.[11,15–17]

A recent theoretical study has shown that the high p-type carrier concentration in SnTe is dominated by the intrinsic negatively charged Sn vacancy (V_{Sn}^{2-}), which always has a negative formation energy regardless of the growth condition, and alloying with Pb can inhibit the formation of cation vacancy.[18] In this paper, additional Pb is used to limit the Sn vacancy. At the same time, alloying with Pb may modify the band structure of SnTe. Different from previous reports, a zone-melting method has been used to synthesize the $SnPb_xTe$ ($x = 0$, 0.02, 0.04, and 0.06) samples. The zone-melting method is widely used in chemical purification, which can lead to purer samples, and it has succeeded in enhancing the electrical properties in layer-structure thermoelectric materials.[19,20] The obtained samples show enhanced power factors ($S^2\sigma$) with a maximum value of 30.5 μW cm^{-1} K^{-2} at 823 K, which is the highest reported value in the SnTe alloys so far. As a result, a maximum ZT of ~0.81 at 823 K is obtained in the p-type $SnPb_{0.04}Te$ sample.

[a]*Ningbo Institute of Materials Technology and Engineering, Chinese Academy of Sciences, Ningbo 315201, China. E-mail: xujingtao@nimte.ac.cn*

[b]*NEST Lab, Department of Chemistry, College of Sciences, Shanghai University, Shanghai 200444, China. E-mail: xujiaqiang@shu.edu.cn*

Experimental

The chemicals: lead (Pb: granule, 1–3 mm 5N), tin (Sn: granule, 1–3 mm 5N) and tellurium (Te: chunk 5N) were used for the synthesis without further purification. The $SnPb_xTe$ (x = 0, 0.02, 0.04, and 0.06) samples were synthesized by mixing appropriate ratios of high purity starting materials of Pb, Sn and Te in a sealed quartz ampoule with an inner diameter of 10 mm under a vacuum (below 10^{-2} Pa). The ampoules were slowly heated to 1123 K over 6 hours, and soaked at this temperature for 2 hours in a rocking furnace to ensure the composition homogeneity, and then cooled to room temperature in the air. These samples were grown in a zone-melting furnace at 1123 K with the growth speed of 25 mm h^{-1}. The density ρ of zone-melted $SnPb_xTe$ alloys was determined using the Archimedes principle. The densities are over 6.36 g cm^{-3} and are higher than those by other methods[11,15–17] (seeing Table S1†). The denser samples may be attributed to the solidification during the zone-melting process, compared to others compressed from powders under high temperature and high pressure. After the zone-melting process, the impurities gather at the beginning or the end of the ingot, due to the different segregation coefficients. Only the middle parts of the zone-melting samples were used for the analysis. 10 × 2 × 2 mm^3 bars and Φ10 × 2 mm^2 plates were cut both along and perpendicular to the growth direction to measure their thermoelectric properties.

The phase compositions of the prepared samples were determined by the powder X-ray diffraction (XRD) analysis using the Cu Kα radiation (λ = 1.5406 Å). The electrical conductivity and Seebeck coefficient were measured by the thermoelectric measurement system (ZEM-3 ULVAC, Japan) under a low-pressure helium atmosphere from room temperature to 823 K. After measuring nine different pieces of one sample, the deviations of the electrical conductivity and Seebeck coefficient were estimated to be within 5% and 7%, respectively (see Fig. S2†). The thermal conductivity was calculated from the values of the thermal diffusivity (λ), the density (ρ) and the specific heat (C_p) by the relationship $\kappa = \lambda\rho C_p$. λ was measured by a laser flash system (Netzsch, LFA-457, Germany) on the plate of Φ10 × 2 mm^2. The heat capacity was determined by $C_p = C_{p,300} + C_{p1} \times ((T/300)^{\alpha} - 1)/((T/300)^{\alpha} + C_{p1}/C_{p,300})$,[21,22] where $C_{p,300}$ is the specific heat capacity at 300 K. During the measurements, the samples were coated with a thin layer of graphite to minimize errors from the emissivity of the materials. The carrier concentration (n) and mobility (μ) were calculated from the Hall coefficient (R_H) which was measured by the physical properties measurement system (PPMS, Quantum Design) in the magnetic fields ranging from 0 to 5 T. Energy dispersive X-ray spectroscopy (EDXS) was performed with the Si (Li) detector of an EDAX system (Gemsis Software V 4.61) to confirm the homogeneous composition of the samples. The composition was calculated from the statistical average of ten different parts of the samples by a standard-less method using the 2 AF matrix correction.

Results and discussions

SnTe has a face-center structure, with a space group of $Fm\bar{3}m$, no. 225 and a lattice parameter of about 6.3 Å at room temperature. The powder X-ray diffraction patterns of the zone-melt samples (x = 0, 0.02, 0.04, and 0.06) are shown in Fig. 1a. All the diffraction peaks are indexed as cubic SnTe (JCPDS card no. 08-0487), and no obvious impurity peak is observed. The main peak of each sample gradually shifts to the lower angle with increasing Pb content, indicating the increase of the lattice constant. The lattice constants of all samples are calculated, and plotted in Fig. 1b. The lattice constant slightly increases from 6.313 Å for x = 0 to 6.324 Å for x = 0.06. The extra Pb atoms (ionic radius ~1.33 Å) can fill the Sn vacancies or substitute Sn atoms (ionic radius ~0.93 Å). They both lead to the expansion of the unit cell. The actual compositions of the zone-melting samples are summarized in Table 1 according to the EDXS results. The actual Pb content of each sample is smaller than the nominal one, which can be understood by the purification nature of the zone-melting method. According to the lattice parameters from the XRD analysis and the real composition of the EDS results, the theoretical density is calculated and listed in Table S1.† The relative density of the samples was above 97.8%, which is also the highest level published so far. For convenience, the nominal Pb contents are used in the following discussions.

The temperature-dependent thermoelectric properties between 300 K and 823 K for the as-prepared bulk materials are plotted in Fig. 2. As shown in Fig. 2a, the electrical conductivity for all samples decreases with increasing the temperature from 300 K to 823 K, showing a typical behavior of the degenerate semiconductor. The electrical conductivity for the sample with x = 0 is ~7900 S cm^{-1} at room temperature, and decreases to ~1900 S cm^{-1} at 823 K, which is consistent with previous reports.[11] With increasing x, the electrical conductivity systematically decreases, indicating that the additional Pb reduces the Sn vacancies. For the sample with x = 0.06, the electrical conductivity is ~6700 S cm^{-1} at room temperature and ~900 S cm^{-1} at 823 K. With the compensation effect of Pb, the electrical conductivity at 823 K decreases more than 50%.

The Hall coefficients of all samples were measured at room temperature. All R_H values are positive, indicating the p-type conduction in this system. The carrier concentration is

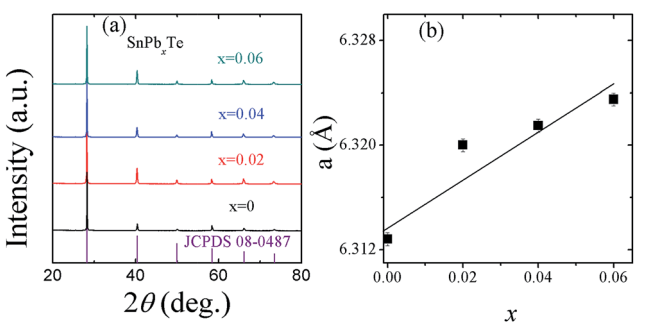

Fig. 1 (a) XRD patterns and (b) lattice parameters for $SnPb_xTe$ samples.

Table 1 The EDS results of the samples: $SnPb_xTe$

x	Sn atom%	Te atom%	Pb atom%
0	51.6 (5)	48.4 (5)	—
0.02	50.0 (2)	48.5 (2)	1.5 (2)
0.04	49.1 (3)	48.5 (2)	2.4 (1)
0.06	47.5 (3)	48.6 (2)	3.9 (3)

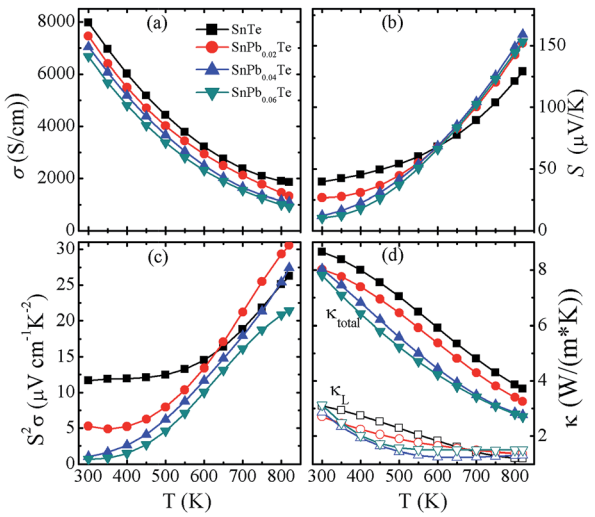

Fig. 2 Temperature dependence of thermoelectric properties for $SnPb_xTe$: (a) electrical conductivity, (b) Seebeck coefficient, (c) power factor, (d) total thermal conductivity (filled points) and lattice thermal conductivity (open points).

estimated using the formula: $n = 1/eR_H$, where e is the electric charge. With increased extra Pb content, the carrier concentration significantly decreases, from 5.77×10^{20} cm^{-3} for $x = 0$ to 1.86×10^{20} cm^{-3} for $x = 0.06$. The result is quite similar to the previous report,[11] indicating that Pb compensation can effectively reduce the Sn vacancies. The hole mobility is estimated by $\mu = \sigma/ne$, and the results are listed in Table 2. The mobility increases with increasing Pb content, from 88 cm^2 V^{-1} s^{-1} for the sample with $x = 0$ to 224 cm^2 V^{-1} s^{-1} for the one with $x = 0.06$. The decrease of the electrical conductivity with extra Pb is dominated by the reduction of the carrier concentration.

The Seebeck coefficients of all samples are shown in Fig. 2b, and are all positive, which is consistent with the Hall coefficient results. With the increasing temperature, the Seebeck coefficient of each sample increases, and does not saturate at 823 K. A "critical" point is found at about 600 K. Below this temperature, the Seebeck coefficient decreases with increasing x, and above this temperature, the Seebeck coefficient increases with increasing x. A similar phenomena has been reported in the Sn-self compensation system.[11]

Table 2 Seebeck coefficient (μV K^{-1}), Hall coefficient (10^{-2} cm^3 C^{-1}), electrical conductivity (10^3 S cm^{-1}), carrier concentration (10^{20} cm^{-3}), carrier mobility (cm^2 V^{-1} s^{-1}), and effective mass (m_e) of all the $SnPb_xTe$ samples at 300 K

x	S	R_H	σ	n	μ	m^*
0	40	1.1	7.97	5.77	88	1.24
0.02	27	1.8	7.45	3.47	134	0.60
0.04	12	2.9	7.03	2.16	204	0.20
0.06	10	3.4	6.66	1.86	224	0.15

At room temperature, the $x = 0$ sample possesses a low Seebeck coefficient of ~40 μV K^{-1}, due to its high hole concentration as mentioned above. The room temperature Seebeck coefficient decreases gradually with the reduction of the hole density, which is opposite from the normal behavior expected for a p-type semiconductor. This anomalous behavior in Seebeck coefficient can be explained by the unique character of the two nondegenerate valence bands of SnTe.[23] In SnTe, the energy difference between the light-hole band at L point and the heavy-hole band at Σ point is around 0.3–0.4 eV.[8–11,22] Owing to the very high hole density in pristine SnTe, the Fermi level is close to the heavy-hole band. With the reduced hole density, the Fermi level rises and gradually shifts away from the heavy-hole band, resulting in the major contribution from the light-hole band to the Seebeck coefficient. The Seebeck coefficient as a function of the hole carrier concentration (Pisarenko plot) at room temperature has been shown in Fig. 3. The dashed line shows the expected room-temperature Seebeck coefficient as a function of hole density for SnTe based on the two nondegenerate valence band model.[10] The Seebeck coefficients of $SnPb_xTe$ samples are slightly above the theoretical Pisarenko curve, indicating Pb compensation hardly changes the band structure of SnTe.

M. Zhou, *et al.* have reported that at room temperature the effective mass for the light band is $0.14m_0$, where m_0 is the mass of free electron, and the one for the heavy band is $1.7m_0$.[21,22] Here, a simple estimation of the effective mass is performed based on a single band assumption. The calculated effective mass decreases from $1.2m_0$ for the pristine SnTe to $0.15m_0$ for the sample with $x = 0.06$, which clearly shows the contribution

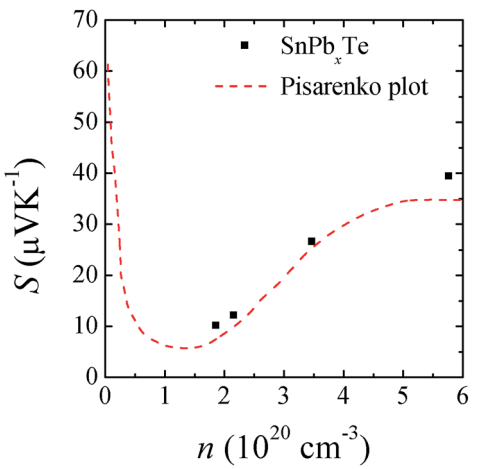

Fig. 3 Room temperature Seebeck coefficient as a function of carrier concentration. The dashed line is a theoretical prediction of the S–n relationship based on a VBM model.[10]

from the heavy band reduces with the carrier concentration decreasing.

At high temperature, the Seebeck coefficient increases with reducing carrier concentration, which probably results from the broadening Fermi distribution and temperature dependent shifts of the band structure.[22] The sample with $x = 0.06$ shows a slightly smaller Seebeck coefficient than that for the one with $x = 0.04$. This may result from a decrease of the band gap due to the introduction of Pb in SnTe.[22,24,25]

Fig. 2c describes the temperature dependence of the power factors ($S^2\sigma$) for all the samples. In the low temperature range (T < 600 K), the power factors deteriorate with increasing Pb content due to both simultaneously decreased electrical conductivities and Seebeck coefficients. At room temperature, it decreases from ~12 μW cm^{-1} K^{-2} for pristine SnTe to 0.69 μW cm^{-1} K^{-2} for the sample with $x = 0.06$. Above 600 K, there is a great enhancement in power factors because of the improvement in the Seebeck coefficients. The pristine SnTe reaches a high power factor of ~26 μW cm^{-1} K^{-2} at 823 K, which benefits from large electrical conductivity (~1900 S cm^{-1}), resulting from the higher density and less other impurities of the middle region of the samples after zone-melting. A maximum power factor value of ~30.5 μW cm^{-1} K^{-2} is obtained at 823 K in the sample with $x = 0.06$, which is the highest value in the SnTe alloys reported so far (see Table 3),[10,11,15,16,22] and could be higher with further increasing the temperature.

The temperature dependence of thermal conductivity for $SnPb_xTe$ samples are presented in Fig. 2d. The total thermal conductivity κ is essentially a combination of two parts: the electronic contribution κ_e and the lattice contribution κ_{lat}. The electronic contribution can be evaluated by the Wiedemann–Franz law:[26] $\kappa_e = L\sigma T$, where L is the Lorenz number, and σ is the electrical conductivity. Here, the L value is obtained from the accepted approach of fitting the Seebeck data to the reduced chemical potential.[27–29] The lattice thermal conductivities are then calculated by subtracting κ_e from κ. The total thermal conductivity values decrease monotonically with increasing x value, caused by the systematic decrease in κ_e. At room temperature, the thermal conductivity decreases from 8.6 W m^{-1} K^{-1} for the pristine SnTe to 7.8 W m^{-1} K^{-1}for the one with $x = 0.06$. There is no definite dependence between κ_{lat} and x, suggesting that the small amount of Pb content in SnTe has little influence on the phonon transport. And the lattice thermal conductivity is from 3.1 W m^{-1} K^{-1} at room temperature to ~1.2 W m^{-1} K^{-1} at 823 K for SnTe. With increased Pb amount, the κ_e/κ ratio at 823 K decreases from 67% for pristine SnTe to 44% for the one with $x = 0.06$.

Table 3 The power factor of the samples SnTe

	Pristine SnTe μW cm^{-1} K^{-2}	Best value μW cm^{-1} K^{-2}
$In_xSn_{1-x}Te$[10]	20@873 K	20@873 K
$Sn_{1.03-x}Cd_xTe$[11]	20.4@770 K	19.5@660 K
$In_xSnTe_{0.85}Se_{0.15}$ (ref. 15)	12.3@710 K	19@855 K
$Sn_{1.03-x}Mg_xTe$[16]	14.2@707 K	30.3@856 K
$Sn_{0.98}Bi_{0.02}Te$–x%$HgTe$[17]	21.8@818 K	27@905 K
This work	26.3@823 K	30.5@823 K

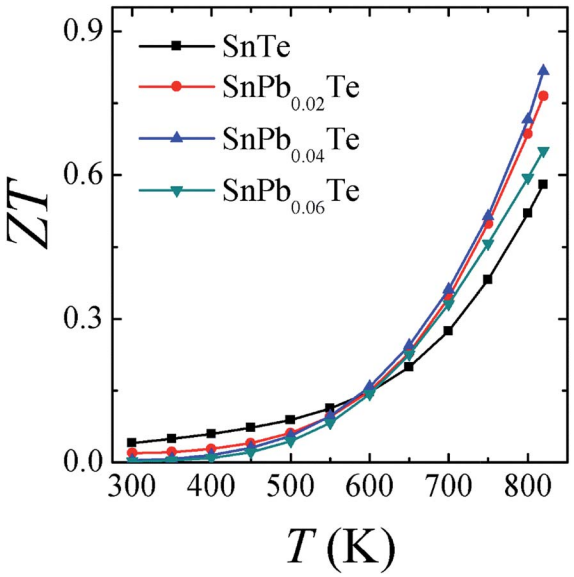

Fig. 4 Temperature dependence of ZT values for SnTe with different Pb contents.

The ZTs as a function of temperature for all the $SnPb_xTe$ compounds are shown in Fig. 4. A ZT value of ~0.6 at 823 K has been obtained in the pristine SnTe, which is about 50% larger than the values reported. This may be due to the larger power factor obtained by the zone-melting method. The highest ZT value of ~0.81 at 823 K was achieved for $SnPb_{0.04}Te$, demonstrating that Pb compensation is effective in suppressing the excessive hole concentration and enhancing the thermoelectric performance of SnTe.

Conclusions

High density alloys of $SnPb_xTe$ (x = 0–0.06) have been synthesized by a zone-melting method. Pb compensation in the SnTe lattice reduces the very high carrier concentration and is very useful to optimize the thermoelectric properties. The zone-melting method enhances the electrical properties, leading to an improved power factor value of ~26.5 μW cm^{-1} K^{-2} at 823 K for the pristine SnTe. A maximum power factor value of ~30.5 μW cm^{-1} K^{-2} is obtained in $SnPb_{0.02}Te$, which is the highest value in the SnTe-based alloys reported so far and could be further improved with increasing temperature. The ZT value is improved from ~0.6 to 0.81 at 823 K by the Pb compensation.

Acknowledgements

This work is supported by the National Nature Science Foundation of China (NSFC no. 11304327, 11404348, 11404350, and 11234012), Ningbo Municipal Natural Science Foundation (2014A610011), and Ningbo Science and Technology Innovation Team (Grant No. 2014B82004).

References

1 H. J. Goldsmid, *Thermoelectric refrigeration*, 1964.
2 L. E. Bell, *Science*, 2008, **321**, 1457–1461.
3 G. Chen, M. Dresselhaus, G. Dresselhaus, J.-P. Fleurial and T. Caillat, *Int. Mater. Rev.*, 2003, **48**, 45–66.
4 D. M. Rowe, *CRC handbook of thermoelectrics*, CRC Press, 1995.
5 J. R. Sootsman, D. Y. Chung and M. G. Kanatzidis, *Angew. Chem., Int. Ed.*, 2009, **48**, 8616–8639.
6 J. P. Heremans, V. Jovovic, E. S. Toberer, A. Saramat, K. Kurosaki, A. Charoenphakdee, S. Yamanaka and G. J. Snyder, *Science*, 2008, **321**, 554–557.
7 J. N. Zemel, J. D. Jensen and R. B. Schoolar, *Phys. Rev.*, 1965, **140**, A330.
8 L. M. Rogers, *J. Phys. D: Appl. Phys.*, 1968, **1**, 845.
9 R. F. Brebrick, *J. Phys. Chem. Solids*, 1963, **24**, 27–36.
10 Q. Zhang, B. Liao, Y. Lan, K. Lukas, W. Liu, K. Esfarjani, C. Opeil, D. Broido, G. Chen and Z. Ren, *Proc. Natl. Acad. Sci. U. S. A.*, 2013, **110**, 13261–13266.
11 G. Tan, L.-D. Zhao, F. Shi, J. W. Doak, S.-H. Lo, H. Sun, C. Wolverton, V. P. Dravid, C. Uher and M. G. Kanatzidis, *J. Am. Chem. Soc.*, 2014, **136**, 7006–7017.
12 Y. Chen, M. D. Nielsen, Y. B. Gao, T. J. Zhu, X. Zhao and J. P. Heremans, *Adv. Energy Mater.*, 2012, **2**, 58–62.
13 G. Tan, F. Shi, H. Sun, L.-D. Zhao, C. Uher, V. P. Dravid and M. G. Kanatzidis, *J. Mater. Chem. A*, 2014, **2**, 20849–20854.
14 A. Banik and K. Biswas, *J. Mater. Chem. A*, 2014, **2**, 9620–9625.
15 A. Banik, U. S. Shenoy, S. Anand, U. V. Waghmare and K. Biswas, *Chem. Mater.*, 2015, **27**, 581–587.
16 G. Tan, F. Shi, J. W. Doak, H. Sun, L.-D. Zhao, P. Wang, C. Uher, C. Wolverton, V. P. Dravid and M. G. Kanatzidis, *Energy Environ. Sci.*, 2015, **8**, 267–277.
17 G. Tan, F. Shi, S. Hao, H. Chi, L.-D. Zhao, C. Uher, C. Wolverton, V. P. Dravid and M. G. Kanatzidis, *J. Am. Chem. Soc.*, 2015, **137**, 5100–5112.
18 N. Wang, D. West, J. Liu, J. Li, Q. Yan, B.-L. Gu, S. Zhang and W. Duan, *Phys. Rev. B: Condens. Matter Mater. Phys.*, 2014, **89**, 045142.
19 Y. Zhai, T. Zhang, Y. Xiao, J. Jiang, S. Yang and G. Xu, *J. Alloys Compd.*, 2013, **563**, 285–288.
20 Y. Xiao, G. Chen, H. Qin, M. Wu, Z. Xiao, J. Jiang, J. Xu, H. Jiang and G. Xu, *J. Mater. Chem. A*, 2014, **2**, 8512–8516.
21 M. Wagner, *These de doctorat*, Universität Wien, 2007.
22 M. Zhou, Z. M. Gibbs, H. Wang, Y. Han, C. Xin, L. Li and G. J. Snyder, *Phys. Chem. Chem. Phys.*, 2014, **16**, 20741–20748.
23 J. A. Kafalas, R. F. Brebrick and A. J. Strauss, *Appl. Phys. Lett.*, 1964, **4**, 93–94.
24 C. W. Li, J. Ma, H. B. Cao, A. F. May, D. L. Abernathy, G. Ehlers, C. Hoffmann, X. Wang, T. Hong, A. Huq, O. Gourdon and O. Delaire, *Phys. Rev. B: Condens. Matter Mater. Phys.*, 2014, **90**, 214303.
25 Y. Tsang and M. L. Cohen, *Phys. Rev. B: Solid State*, 1971, **3**, 1254.
26 A. Bejan and A. D. Kraus, *Heat transfer handbook*, Wiley, New York, 2003.
27 S. Johnsen, J. He, J. Androulakis, V. P. Dravid, I. Todorov, D. Y. Chung and M. G. Kanatzidis, *J. Am. Chem. Soc.*, 2011, **133**, 3460–3470.
28 A. F. May, J.-P. Fleurial and G. J. Snyder, *Phys. Rev. B: Condens. Matter Mater. Phys.*, 2008, **78**, 125205.
29 S. N. Girard, J. He, X. Zhou, D. Shoemaker, C. M. Jaworski, C. Uher, V. P. Dravid, J. P. Heremans and M. G. Kanatzidis, *J. Am. Chem. Soc.*, 2011, **133**, 16588–16597.